Journal of Computational and Applied Mathematics 234 (2010) 2143–2151

Contents lists available at ScienceDirect

Journal of Computational and Applied Mathematics

journal homepage: www.elsevier.com/locate/cam

Dam break flow computation based on an efficient flux vector splitting

S. Erpicum [a], B.J. Dewals [a,b], P. Archambeau [a], M. Pirotton [a,*]

[a] HACH Research Unit, ArGEnCo Department, University of Liège, Chemin des Chevreuils, 1 B52/3, B-4000 Liège, Belgium

[b] Belgian National Fund for Scientific Research F.R.S-FNRS, Belgium

ARTICLE INFO

Article history:
Received 15 September 2008
Received in revised form 9 February 2009

Keywords:
Dam break flow
Shallow-water equations
Flux vector splitting

ABSTRACT

Dam break flow computation is a task of prime interest in the scope of risk analysis processes related to dams and reservoirs. In this paper, a 2D finite volume multiblock flow solver, able to deal with natural topography variation, is presented in detail. The model is based on an efficient Flux Vector Splitting method developed by the authors. A number of validation examples are comprehensively described.

1. Introduction

Dams and reservoirs are recognized for their valuable contribution to the prosperity and wealth of societies across the world, while they are also blamed for their risk of failure. Failures of large dams remain fortunately very seldom events. Nevertheless, a number of occurrences have been recorded in the world, corresponding in average to one to two failures worldwide every year. Some of those accidents have caused catastrophic consequences, but past experience reveals also that loss of life and damage can be drastically reduced if Emergency Action Planning (EAP) is implemented in the downstream valley. The development of EAP is an outcome of a complete risk analysis process, which requires, among other components, a detailed prediction of the propagation of the flood wave induced by the dam failure.

In this general scope, since practical risk analysis must be applicable for long real valleys at a sufficiently high space resolution, depth-averaged hydrodynamic models still constitute the most appealing approach [1]. Nevertheless, numerical modelling of such flows involves numerous challenges to be taken up. First, the flow is characterized by a highly transient behaviour involving the propagation of stiff fronts. Therefore, a proper upwind numerical scheme is required for the computation to be stable, while a satisfactory accuracy must be reached in space and time. Secondly, conservation of physical quantities must be preserved during wetting and drying of computation cells. Finally, the hydrodynamic model must be able to deal with flows over natural topographies, which are inherently irregular. The correct computation of momentum and energy quantities requires a suitable discretization of the source term representing the bottom slope.

Many authors such as Fread [2], Bellos and Sakkas [3], Glaister [4], Fennema and Chaudhry [5] or Alcrudo and al. [6] have shown early interest in dam break flow numerical computation. Various techniques have been developed to solve the 1D flow equations, as shown in [7]. In the early nineties, research was conducted at the University of Liege in [8], leading to a 1D upwind finite element scheme to compute dam break flows on natural topography and to its validation by physical modelling. The simulation time exceeded one week to run on 200 cells. Today, the corresponding 2D model is run in less than

* Corresponding address: ArGEnCo Department, Research unit of Applied Hydrodynamics and Hydraulic Constructions, University of Liege, Chemin des Chevreuils, 1 B52/3, B-4000Liege, Belgium.

E-mail addresses: S.Erpicum@ulg.ac.be (S. Erpicum), B.Dewals@ulg.ac.be (B.J. Dewals), Pierre.Archambeau@ulg.ac.be (P. Archambeau), Michel.Pirotton@ulg.ac.be (M. Pirotton).

0377-0427/$ – see front matter © 2009 Elsevier B.V. All rights reserved.
doi:10.1016/j.cam.2009.08.110

one day on a 200,000-cell grid. Based on a finite volume scheme, this 2D hydrodynamic model handles multiblock regular grids and a specific iterative process to simulate wetting and drying of computation cells without mass or momentum error. Following extensive validation by comparison with theoretical, experimental and field data [9,10], this 2D model has proved its efficiency and reliability for open channel flow computations. In this paper, it is specifically applied to dam break flow computation.

2. Hydraulic model description

2.1. Mathematical model

The 2D hydraulic model is based on the 2D depth-averaged equations of volume and momentum conservation, namely the shallow-water equations (SWE). In the standard shallow-water approach, the only assumption states that vertical velocities are significantly smaller than horizontal ones. As a consequence, the pressure field is found to be almost hydrostatic everywhere. The large majority of flows occurring in natural valleys, even highly transient, can be reasonably seen as shallow, except in the vicinity of some singularities (e.g. weirs). Indeed, vertical velocity components remain generally low compared to velocity components in the horizontal plane and, consequently, flows may be considered as mainly 2D. Thus, the approach presented in this paper is suitable for many of the problems encountered in river management as well as for dam break modelling.

The conservative form of the depth-averaged equations of mass and momentum conservation can be written as follows, using vector notations:

$$\frac{\partial \mathbf{s}}{\partial t} + \frac{\partial \mathbf{f}}{\partial x} + \frac{\partial \mathbf{g}}{\partial y} + \frac{\partial \mathbf{f}_d}{\partial x} + \frac{\partial \mathbf{g}_d}{\partial y} = \mathbf{S}_0 - \mathbf{S}_f \tag{1}$$

where $\mathbf{s} = [h\ hu\ hv]^{\mathrm{T}}$ is the vector of the conservative unknowns. Vectors $\mathbf{f}$ and $\mathbf{g}$ represent the advective and pressure fluxes in directions x and y, while $\mathbf{f}_d$ and $\mathbf{g}_d$ are the diffusive fluxes:

$$\begin{gathered} \mathbf{f} = \begin{pmatrix} hu \\ hu^2 + \frac{1}{2}gh^2 \\ huv \end{pmatrix}, \qquad \mathbf{g} = \begin{pmatrix} hv \\ huv \\ hv^2 + \frac{1}{2}gh^2 \end{pmatrix}, \\ \mathbf{f}_d = -\frac{h}{\rho}\begin{pmatrix} 0 \\ \sigma_x \\ \tau_{xy} \end{pmatrix}, \qquad \mathbf{g}_d = -\frac{h}{\rho}\begin{pmatrix} 0 \\ \tau_{xy} \\ \sigma_y \end{pmatrix}. \end{gathered} \tag{2}$$

$\mathbf{S}_0$ and $\mathbf{S}_f$ designate respectively the bottom slope and the friction terms:

$$\mathbf{S}_0 = -gh\,[0\ \partial z_b/\partial x\ \partial z_b/\partial y]^{\mathrm{T}} \qquad \mathbf{S}_f = \left[0\ \tau_{bx}\Delta\Sigma/\rho\ \tau_{by}\Delta\Sigma/\rho\right]^{\mathrm{T}}. \tag{3}$$

In Eqs. (1)–(3), t represents the time, x and y the space coordinates, h the water depth, u and v the depth-averaged velocity components, z_b the bottom elevation, g the gravity acceleration, ρ the density of water, τ_{bx} and τ_{by} the bottom shear stresses, σ_x and σ_y the turbulent normal stresses and τ_{xy} the turbulent shear stresses. Consistently with Hervouet [11],

$$\Delta\Sigma = \sqrt{1 + (\partial z_b/\partial x)^2 + (\partial z_b/\partial y)^2} \tag{4}$$

reproduces the increased friction area on an irregular (natural) topography [12].

2.2. Friction modelling

The bottom friction is conventionally modelled thanks to an empirical law, such as the Manning formula. The model enables the definition of a spatially distributed roughness coefficient to represent different land-uses, floodplain vegetations or sub-grid bed forms . . . Besides, the model provides the additional possibility to reproduce friction along the side walls by means of a process-oriented formulation [9,12]. The combined effect of bottom and side wall friction is expressed as:

$$\begin{aligned} \frac{\tau_{bx}}{\rho} &= ghu\left[\sqrt{u^2+v^2}\,\frac{n_b^2}{h^{4/3}} + u\sum_{k_x=1}^{N_x}\frac{4}{3}\frac{n_W^2}{h^{1/3}\Delta y}\right] \\ \frac{\tau_{by}}{\rho} &= ghv\left[\sqrt{u^2+v^2}\,\frac{n_b^2}{h^{4/3}} + v\sum_{k_y=1}^{N_y}\frac{4}{3}\frac{n_W^2}{h^{1/3}\Delta x}\right] \end{aligned} \tag{5}$$

where the Manning coefficient n_b and n_w characterize respectively the bottom and the side walls roughness and N_x and N_y designate the number of edges of the finite volume cell which are in contact with the side wall. Those relations are particularized for Cartesian grids exploited in the present study.

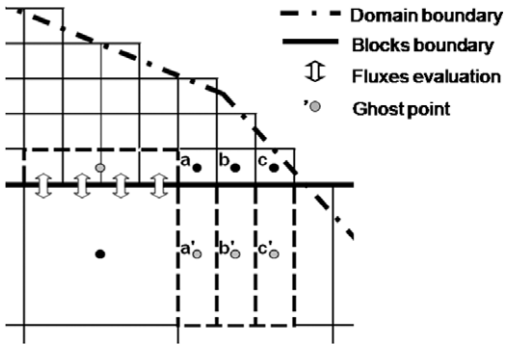

Fig. 1. Border between two adjacent blocks on a Cartesian multiblock grid.

The internal friction should be reproduced by applying a proper turbulence model. Several ones were implemented and tested in the solver, starting from rather simple algebraic expressions of turbulent viscosity to a depth-integrated $k-\varepsilon$ type model involving additional partial differential equations [13]. For the computations presented in this paper, no turbulence model has been used due to the mainly advective behaviour of dam break induced flows. All friction effects are thus globalized in the bottom and wall friction term in a fitted value of the roughness coefficient.

2.3. Grid and numerical scheme

The solver includes a mesh generator and deals with multiblock grids. Within each block, the grid is Cartesian. The main advantages of this type of structured regular grids compared to nonregular ones are the lower computation time and the gain in accuracy as a result of error compensations. To overcome the main problem of Cartesian grids, i.e. the high number of cells needed for a fine enough discretization, multiblock features can increase the domain areas that can be discretized with a constant number of cells and enable local mesh refinements near areas of interest. In addition, to decrease the number of computation elements at each time step, an automatic grid adaptation procedure restricts the simulation domain to the wet cells and a surrounding narrow strip of dry volumes. Besides, wetting and drying of cells is handled free of volume and momentum conservation errors by the way of an iterative resolution of the continuity equation prior to any evaluation of the momentum equations [13].

The space discretization of Eq. (1) is performed by means of a finite volume scheme. This ensures a proper mass and momentum conservation, which is a prerequisite for handling reliably discontinuous solutions such as moving hydraulic jumps. As a consequence, no assumption is required as regards the smoothness of the solution. Reconstruction at cell interfaces can be performed constantly or linearly, in conjunction with slope limiting, leading in the later case to a second order spatial accuracy. In a similar way, variables at the border between adjacent blocks are reconstructed linearly, using in addition ghost points as depicted in Fig. 1. The variables at the ghost points are evaluated from the value of the subjacent cells. Moreover, to ensure conservation properties at the border between adjacent blocks and thus to compute accurate volume and momentum balances, fluxes related to the larger cells are computed at the level of the finer ones.

Achieving consistency between flux computation and source terms evaluation has always been a challenging issue in computational fluid dynamics. The fluxes $\mathbf{f}$ and $\mathbf{g}$ are computed by a Flux Vector Splitting (FVS) method developed by the authors. Following this FVS, the upwinding direction of each term of the fluxes is simply dictated by the sign of the flow velocity reconstructed at the cell interfaces. It can be formally expressed as follows:

$$\mathbf{f}^{+}=\begin{pmatrix} hu \\ hu^2 \\ huv \end{pmatrix}, \qquad \mathbf{f}^{-}=\begin{pmatrix} 0 \\ \frac{1}{2}gh^2 \\ 0 \end{pmatrix}$$
$$\mathbf{g}^{+}=\begin{pmatrix} hv \\ huv \\ hv^2 \end{pmatrix}, \qquad \mathbf{g}^{-}=\begin{pmatrix} 0 \\ 0 \\ \frac{1}{2}gh^2 \end{pmatrix} \tag{6}$$

where the exponents $+$ and $-$ refer to, respectively, an upstream and a downstream evaluation of the corresponding terms. A Von Neumann stability analysis has demonstrated that this FVS leads to a stable spatial discretization of the terms $\frac{\partial \mathbf{f}}{\partial x}$ and $\frac{\partial \mathbf{g}}{\partial y}$ in Eq. (1) [12]. Due to their diffusive nature, the fluxes $\mathbf{f}_d$ and $\mathbf{g}_d$ are legitimately evaluated by means of a centred scheme.

Besides requiring a low computation cost, this FVS offers the advantages of being completely Froude independent and of facilitating a satisfactory adequacy with the discretization of the bottom slope term. This FVS has already proved its validity and efficiency for numerous applications [9,10].

2.4. Topography gradients

The discretization of the topography gradients is also a challenging task when setting up a numerical flow solver based on the SWE. The bed slope appears as a source term in the momentum equations. As a driving force of the flow, it has however to be discretized carefully, in particular regarding the treatment of the advective terms leading to the water movement, such as pressure and momentum.

In the model presented in this paper, according to the FVS characteristics, a suitable treatment of the topography gradient source term of Eq. (4) is a downstream discretization of the bottom slope and a mean evaluation of the corresponding water heights [13]. For a mesh i and considering a constant reconstruction of the variables, the bottom slope discretization writes:

$$-gh\frac{\partial z_b}{\partial x, y}|_i \longrightarrow -g\frac{(h|_{i+1} - h|_i)}{2}\frac{\partial\,(z_b|_{i+1} - z_b|_i)}{\partial x, y} \tag{7}$$

where subscript $i + 1$ refers to the downstream mesh along x- or y-axis.

This approach fulfils the numerical compatibility conditions defined in [14] regarding the stability of water at rest. The final formulation is the same as the one proposed in [15] or [16]. It is suited to be used in both 1D and 2D models, along x- and y-axis. Its very light expression benefits directly from the simplicity of the original spatial discretization scheme.

Nevertheless, the formulation of Eq. (7) constitutes only a first step towards an adequate form of the topography gradient as it is not entirely suited regarding water in movement over an irregular bed. The effect of kinetic terms is not taken into account and, as a consequence, inaccurate evaluation of the flow energy evolution can occur when modelling flow over a variable topography [13].

2.5. Time discretization and boundary conditions

Since the model is applied to transient flows and flood waves, the time integration is performed by means of a second order accurate and hardly dissipative explicit Runge–Kutta (RK) method. For stability reasons, the time step is constrained by the Courant–Friedrichs–Levy (CFL) condition based on gravity waves. A semi-implicit treatment of the bottom friction term is used, without requiring additional computational costs.

For each application, the value of the specific discharge can be prescribed as an inflow boundary condition. Besides, the transverse specific discharge is usually set to zero at the inflow even if its value can also be prescribed to a different value if necessary. In case of supercritical flow, a water elevation can be provided as additional inflow boundary condition. The outflow boundary condition may be a water surface elevation, a Froude number or no specific condition if the outflow is supercritical. At solid walls, the component of the specific discharge normal to the wall is set to zero. In case of dam break flow modelling, no boundary condition is generally needed in the model as the flows in the reservoir and the downstream valley are bounded by the natural topography.

3. Model validation

3.1. Mobile hydraulic jump

As a first test case, the propagation of a moving hydraulic jump in a smooth and horizontal channel with a constant rectangular cross-section has been considered. In such a particular channel, considering a hydraulic jump moving with constant velocity along the channel axis, the mass and momentum equations provides analytical data for the validation of the numerical approach.

The computation has been performed considering a 50 m long and 3 m wide channel. No friction has been taken into account on the bottom or the side walls. The velocity of the hydraulic jump is 2 m/s and the water depth is 1 m upstream and 5 m downstream of the discontinuity. Thus, the specific discharges have to be 14.13 and 22.12 m^2/s respectively upstream and downstream of the hydraulic jump for the amplitude of the shock to be constant along time. Upstream boundary conditions are the specific discharge and the water depth (supercritical flow) and the downstream condition is the water depth (subcritical flow). The initial condition corresponds to an instantaneous hydraulic jump location 4.5 m from the upstream limit of the channel.

The channel has been discretized with a multiblock grid made of two 15 m long reaches with a 0.5 m mesh size on either side of a central reach 20 m long with coarse meshes of 1 m. Flux reconstruction is constant inside a block and linear at the boundaries. Thus, the discretization scheme is first order accurate. The time integration scheme is second order accurate ($\mathrm{RK22} - \mathrm{CFL} = 0.2$).

The computation has been carried out for a period of 20 s. This allows the hydraulic jump to cover the most of the channel length and to cross twice a boundary between blocks.

The comparison between the instantaneous analytical and numerical free surface levels is satisfactory (Fig. 2). The velocity of the moving shock and its amplitude are very well reproduced along the whole channel, even across the block boundaries. The effect of the linear reconstruction at the block boundary is visible with a local stiffening of the shock, but the instantaneous hydraulic jump profile remains very similar inside the three blocks.

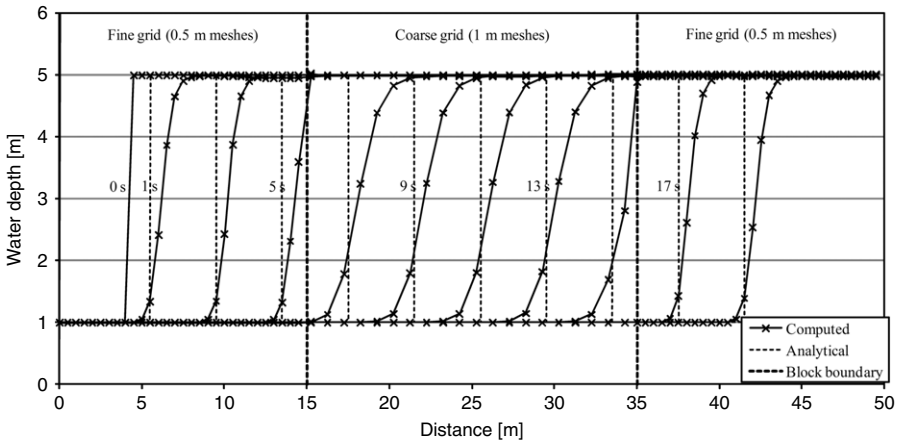

Fig. 2. Propagation of a mobile hydraulic jump in a smooth horizontal channel — Analytical and numerical results with multiblock grid.

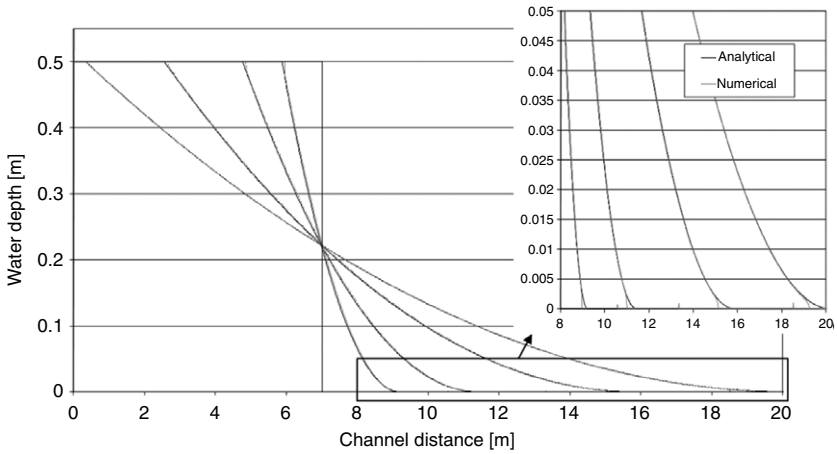

Fig. 3. Analytical and numerical free surface profiles near the front after 0, 0.5, 1, 2 and 3 s of propagation.

3.2. Dam break wave on a smooth dry bed

Under the assumption of shallow water, the analytical calculation of the dam break wave propagation on smooth dry bed has been performed for the first time by Ritter. This test case has been used as a second application to assess the accuracy of the numerical scheme and to validate the automatic grid adaptation procedure.

A straight channel 20 m long has been modelled with 2000 cells of 0.01 m. The bed is horizontal and the bottom and wall friction is set to 0. At time zero, a 0.5 m high water volume on the 7 first meters of the channel is released instantaneously. A propagation wave moves downwards while a rarefaction wave goes back in the reservoir. The numerical computation has been performed with a second order accurate space and time integration scheme (RK 22 and linear reconstruction with slope limitation). The CFL number was 0.4.

The numerical results are compared with the analytical solution on the first three seconds of propagation (Fig. 3). The successive free surface profiles are perfectly articulated around the critical depth at the initial front location and the wave propagation is accurately reproduced both upstream and downstream.

3.3. Circular dam break

The third test case consists in computing the flow induced by the instantaneous collapse of an idealized circular dam, as initially described in [17]. A cylindrical dam with radius equal to 11 m is considered, separating the computational domain into an inner and an external area, with respective initial water depths of 10 m and 1 m, and zero discharge. The bed is horizontal, while the bed friction is neglected. The dam is removed at time $t = 0$.

Since the problem is actually 1D along the radial direction, a reference solution obtained from a 1D computation on a very fine grid may be used to compare with the results of the 2D simulations. The test case enables to verify, on one hand, the ability of the model to represent the 2D propagation of unsteady stiff waves and, on the other hand, to check the capacity of the model to preserve symmetry within the numerical solution.

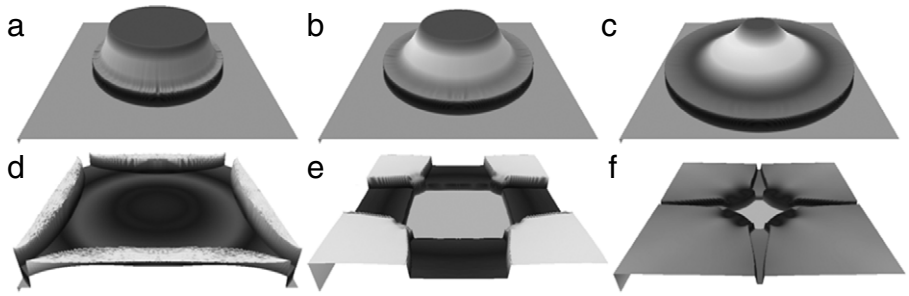

Fig. 4. Instantaneous 3D views of the free surface at 4 different time steps following the sudden collapse of an idealized circular dam: (a) 0.2 s, (b) 0.4 s, (c) 0.8 s, (d) 1.8 s, (e) 3.6 s and (f) 4.5 s.

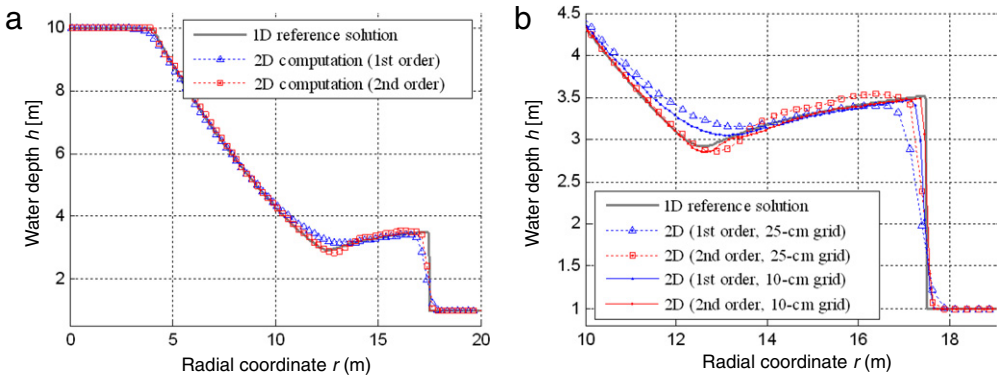

Fig. 5. Computed water depths after 0.69 s for the flow induced by the collapse of a circular dam. 1D reference solution as well as 2D solutions obtained with schemes first and second order accurate in space: (a) 0.25m cells ; (b) details of 0.25m and 0.10m cells.

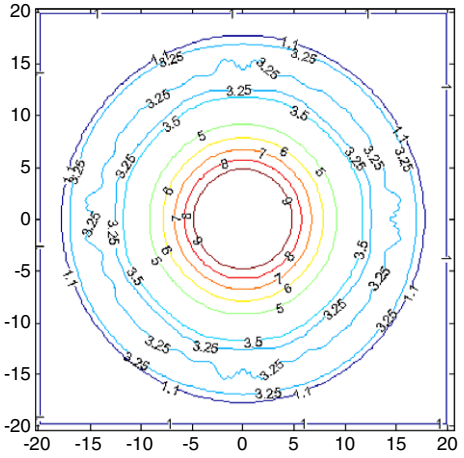

Fig. 6. Contour lines of the free surface (m) after 0.69 s for the flow induced by the circular dam break. Details of the variations close to the shock.

The reference solution is obtained by solving the 1D formulation of the continuity and momentum equations, written as a function of a radial coordinate and considering the rotational symmetry [12]. The system has been solved on a fine mesh (2000 elements), based on a finite volume scheme second order accurate both in space and time (RK22 and linear reconstruction with slope limitation).

2D simulations have been conducted on a single block with cells of 0.25 m, as well as on a finer mesh (0.10 m cells). The time integration is performed with the same numerical scheme.

Fig. 4 illustrates the free surface obtained at four successive times. The solution involves a shock propagating towards outside and a rarefaction wave propagating towards inside. It must be noted that, in contrast with the Stoker solution, the part of the solution immediately upstream of the shock is not a horizontal platform anymore, as a result of the 2D behaviour of the flow.

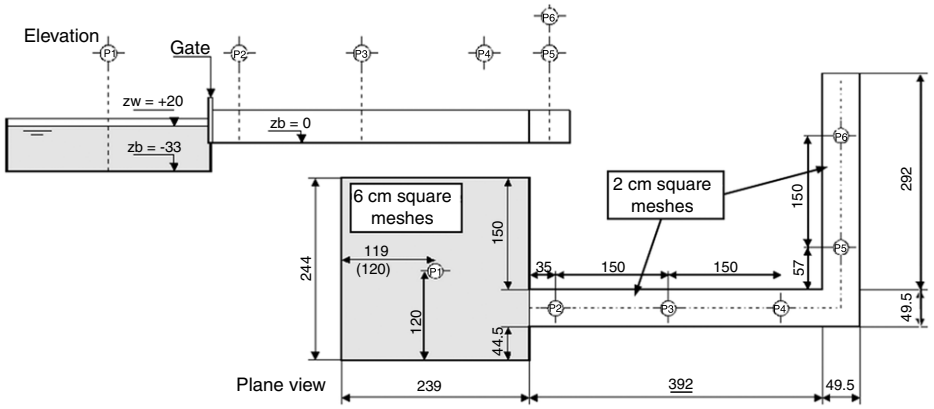

Fig. 7. Experimental facility for the L-channel test (dimensions in cm) and numerical discretization features.

Fig. 5 shows the satisfactory agreement between the radial distributions of water depth in the reference solution and the one predicted by the computation. For comparison purpose, the 2D simulations have been conducted with either a first or a second order accurate space discretization. The overall shock propagation is faithfully reproduced by both schemes, while the second order scheme achieves slightly better results at both sides of the rarefaction wave as well as in the vicinity of the shock, as a result of its weaker numerical diffusion. Although refining the grid obviously contributes to improve the solution, the second order space discretization on the 0.25 m mesh performs almost as well as it does on the finer mesh.

Different authors have studied the circular dam break problem on structured polar grids [17,18], which enable to preserve the cylindrical symmetry of the solution. In contrast, computations performed on Cartesian grids show some influence of the axes of reference on the wave propagation [17,18] and simulations based on unstructured grids, such as triangular cells, are unable to preserve the cylindrical symmetry exactly [19]. In the present case, the contour lines displayed in Fig. 6 highlights precisely the achieved rotational symmetry of order four, which is actually the best level of symmetry possible to be reached exactly on a Cartesian grid.

3.4. Dam break in an L-channel

To assess the efficiency of the numerical model to compute dam break induced waves in nonstraight channels, the L-channel experimental benchmark of the European CADAM Project [20] has been considered as a second 2D validation example.

The experimental facility, built at the University of Leuven (UCL) in Belgium consists in a square reservoir upstream of two rough horizontal channel reaches linked by a 90 deg bend (Fig. 7). The channel cross-section is rectangular. The downstream reach extremity is a free overflow. A 0.33 m high topography step is located between the reservoir and the first reach. A guillotine type gate separates the reservoir and the channel. At time zero, the gate is almost instantaneously lifted and a wave propagates into the channel reaches, with partial reflection on the 90 deg bend. The experimental facility is equipped with 6 gauges measuring the water depth evolution during 20 s with a frequency of 0.1 s.

Preliminary numerical tests suggested a roughness coefficient equal to 0.006 $s/m^{1/3}$ for both the steel bottom and the glass side walls. The simulation has been performed with a first order accurate space discretization scheme and a second order accurate time integration scheme (RK 22 − CFL = 0.1). The grid for numerical modelling is based on 0.02 m square meshes in the channel reaches and 6 cm ones in the reservoir (Fig. 7).

The curves of Fig. 8 show the unsteady evolution of the water depths in the reservoir and the channel reaches at gauges P1, P3 and P5 in both the experimental facility and the numerical model. The numerical results are in very good agreement with the experimental ones.

3.5. Bump

Finally, the CADAM test case of the dam break flow propagation in a rough channel with a bump [21] has been used to test the model on an irregular topography. In addition, for the first seconds of the propagation, the experimental and numerical results can be compared with the Dressler analytical solution for the propagation on a dry rough horizontal bed. The experimental setup (Fig. 9), realized at the Laboratory of Hydraulic Research of Chatelet in Belgium, consists in a straight channel 38 m long and 0.75 m wide. A topography variation (bump) is located 10 m downstream of a plate retaining a 0.75 m deep and 15.50 m long water volume. The symmetric bump is 6 m long and 0.4 m high. Upstream of the bump, the channel is dry while it is filled with a 0.15 m deep water surface downstream. The channel extremities are impermeable. The experimental test consists in removing the plate in a very short time (0.5 s) and measuring the wave propagation along the channel with several probes during 60 s with a frequency of 0.1 s.

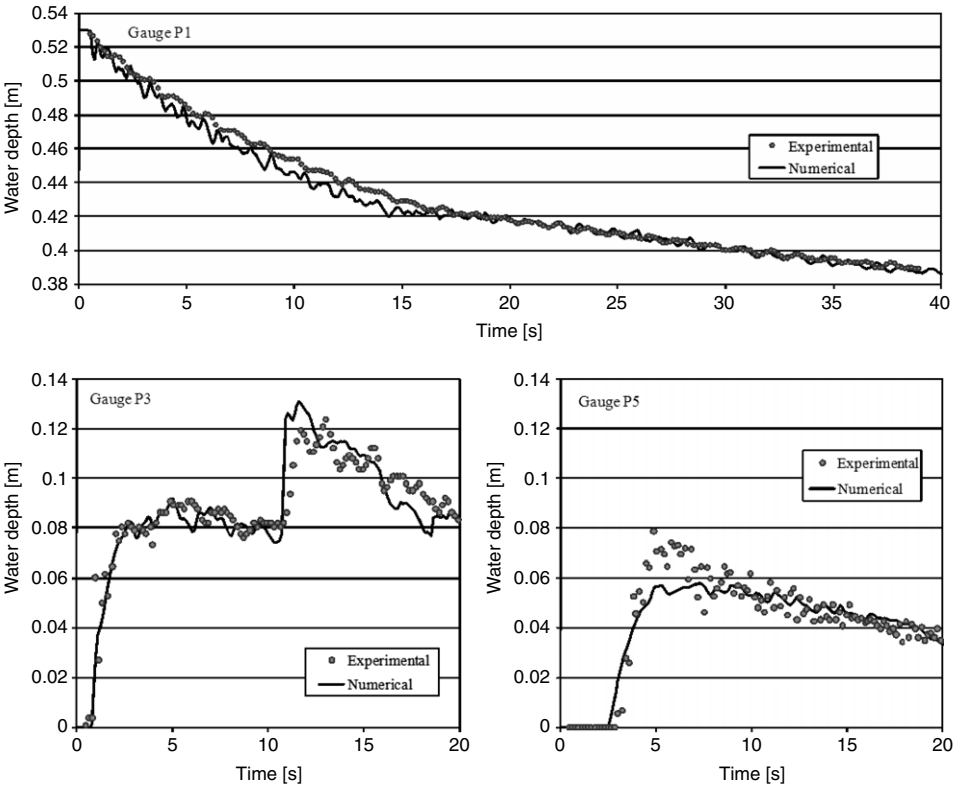

Fig. 8. Experimental and numerical results at gauges P1, P3 and P5 of the L-channel.

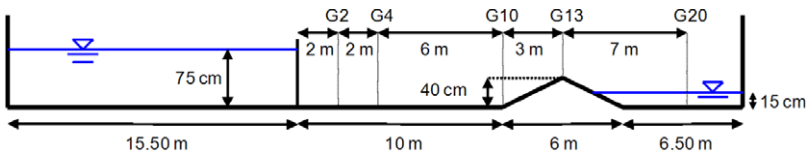

Fig. 9. Scheme of the experimental installation for the bump test case.

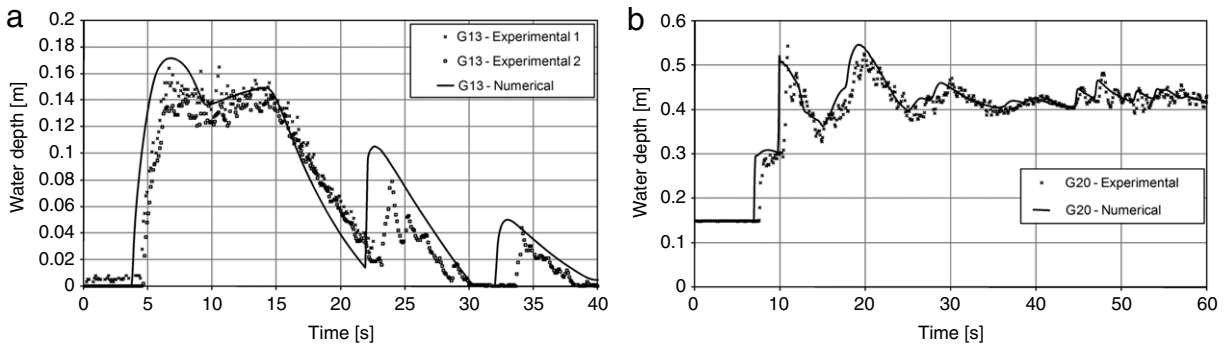

Fig. 10. Analytical, experimental and numerical results at gauges G13 (a) and G20 (b) in the bump channel.

The computation has been performed using a uniform 5 cm grid (RK22 – CFL0.4). The best value for both wall and bottom friction have been found by calibration to be 0.0085 $s/m^{1/3}$.

The numerical results show satisfactory agreement with the experimental ones upstream, on and downstream of the bump (Figs. 10 and 11). The wave partial reflection, propagation times and amplitudes are well reproduced by the numerical scheme in the whole simulation domain, as well as the temporary drying at the bump peak (Fig. 10a). At gauge G4, the numerical results are concordant with the analytical solution and the time shifting between the numerical and the experimental results is in the order of magnitude of the plate removing time (Fig. 11).

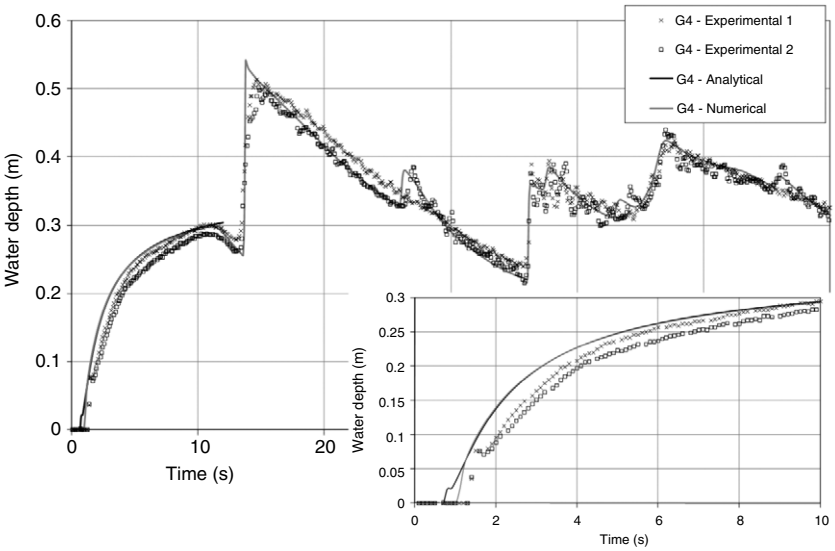

Fig. 11. Analytical, experimental and numerical results at gauges G4 in the bump channel.

4. Conclusion

Depth-averaged hydrodynamic models constitute a realistic numerical approach for accurate and finely distributed computation of dam break wave propagation. Such a model is presented in detail in this paper. It is based on an efficient Flux Vector Splitting method developed by the authors and deals with multiblock regular grids. Its particular features enable a stable and accurate flow computation, even on irregular wetting–drying topography, with an exact conservation of the mass and momentum quantities.

References

[1] V. Caleffi, A. Valliani, A. Zanni, Finite volume method for simulating extreme flood events in natural channels, Journal of Hydraulic Research 41 (2) (2003) 167–177.
[2] D.L. Fread, DAMBRK: The NWS dam break flood forecasting model, National Weather Service (NWS) Report, Silver Spring, MA, USA, 1984.
[3] C.V. Bellos, J.G. Sakkas, 1-D dam-break floow-wave propagation on dry bed, Journal of Hydraulic Engineering—ASCE 113 (12) (1987) 1510–1524.
[4] P. Glaister, Approximate Riemann solutions of the shallow water equations, Journal of Hydraulic Research 26 (3) (1988) 293–300.
[5] R.J. Fennema, M.H. Chaudhry, Explicit methods for 2-D transient free surface flows, Journal of Hydraulic Engineering—ASCE 116 (8) (1990) 1013–1034.
[6] F. Alcrudo, P. Garcia-Navarro, J-M. Saviron, Flux difference splitting for 1D open channel flow equations, International Journal of Numerical Methods in Fluids 14 (9) (1992) 1009–1018.
[7] P. Garcia-Navarro, A. Fras, I. Villanueva, Dam-break flow simulation: Some results for one-dimensional models of real cases, Journal of Hydrology 216 (1999) 227–247.
[8] M. Pirotton, Modélisation des discontinuités en écoulement instationnaire à surface libre. Du ruissellement hydrologique en fine lame à la propagation d'ondes consécutives aux ruptures de barrages, Ph.D. Thesis, University of Liege, 1994.
[9] S. Erpicum, T. Meile, B.J. Dewals, M. Pirotton, A.J. Schleiss, 2D numerical flow modeling in a macro-rough channel, International Journal of Numerical Methods in Fluids 61 (11) (2009) 1227–1246.
[10] B.J. Dewals, S.A. Kantoush, S. Erpicum, M. Pirotton, A.J. Schleiss, Experimental and numerical analysis of flow instabilities in rectangular shallow basins, Environ. Fluid Mech. 8 (2008) 31–54.
[11] J.-M. Hervouet, Hydrodynamique des écoulements à surface libre Modélisation numérique avec la méthode des éléments finis, Presses de l'école nationale des Ponts et Chaussées, Paris, 2003.
[12] B.J. Dewals, Une approche unifiée pour la modélisation d'écoulements à surface libre, de leur effet érosif sur une structure et de leur interaction avec divers constituants, Ph.D. Thesis, University of Liege, 2006.
[13] S. Erpicum, Optimisation objective de paramètres en écoulements turbulents à surface libre sur maillage multibloc, Ph.D. Thesis, University of Liege, 2006.
[14] M. Nujic, Efficient implementation of non-oscillatory schemes for the computation of free surface flows, Journal of Hydraulic Research 33 (1) (1995) 101–111.
[15] S. Soares Frazao, Dam-break induced flows in complex topographies, Theoretical, numerical and experimental approaches, Ph.D. Thesis, Université Catholique de Louvain, 2000.
[16] E. Audusse, Modélisation hyperbolique et analyse numérique pour les écoulements en eaux peu profondes, Ph.D. Thesis, Université Paris VI Pierre et Marie Curie, 2004.
[17] F. Alcrudo, P. Garcia-Navarro, A high resolution Godunov-type scheme in finite volumes for the 2D shallow-water equations, International Journal of Numerical Methods in Fluids 16 (1993) 489–505.
[18] C. Mingham, D. Causon, High-resolution finite volume method for shallow water flows, Journal of Hydraulic Engineering—ASCE 124 (6) (1998) 605–614.
[19] K. Anastasiou, C. Chan, Solution of the 2D shallow water equations using finite volume method on unstructured triangular meshes, International Journal of Numerical Methods in Fluids 24 (1997) 1225–1245.
[20] S. Soares Frazo, Y. Zech, Dam-break in channels with 90 bend, Journal of Hydraulic Engineering—ASCE 128 (11) (2002) 956–968.
[21] F. Alcrudo, S. Soares Frazo, Conclusions from the 1st CADAM meeting, in: CADAM Proceedings—Wallingford meeting, 1998. URL: http://www.hrwallingford.co.uk/projects/CADAM/CADAM/index.html.